# Microstructure and Corrosion Properties of ZK60 Alloys Modified by Micro-Arc Oxidation Coatings Using Phosphate-Borate Electrolyte in KOH Solution

*Shangjun Ma[1,2], Taolei Wang[2], Liwei Qian[2], Zhen Xiang[2], Wei Lu[2] and Huawei Yang[1,\*]*

[1] Department of Stomatology, Affiliated Shanghai Tenth People's Hospital, Tongji University, Shanghai 200072 China
[2] School of Materials Science and Engineering, Shanghai Key Laboratory of D&A for Metal-Functional Materials, Tongji University, Shanghai 201804, China
[\*]E-mail: yanghuawei@tongji.edu.cn

In this work, $Na_3PO_4$ (0.05 M) and $Na_2B_4O_7$ (0.02 M) were used as basic electrolytes for fabricating micro-arc oxidation coatings on ZK60 magnesium alloy. The effects of KOH concentrations (0.01, 0.05, and 0.1 M) on microstructure, chemical composition, and corrosion resistance were systematically investigated. The results revealed that MAO-coated samples prepared in 0.05 M aqueous KOH possessed relatively low thickness (8.82 µm), small pore size (3.33 µm), and the lowest porosity ($5.156 \times 10^{-3}$ pores/$\mu m^2$). Also, there were no evident microcracks in MAO coatings prepared in 0.05 M aqueous KOH and the pore distribution was uniform. The resulting corrosion characteristics of MAO-coated ZK60 alloys in simulated body fluid solution (SBF) were significantly affected by the KOH concentration. ZK60 alloy coated with MAO prepared in 0.05 M KOH had relatively high self-corrosion potential (-1.28 V), highest polarization resistance (2667.23 k$\Omega \cdot cm^2$), lowest corrosion current density ($4.36 \times 10^{-7}$ A$\cdot cm^{-2}$), and low corrosion rate ($1.00 \times 10^{-5}$ mm$\cdot yr^{-1}$), indicating the highest corrosion resistance in SBF and suggesting that MAO coatings prepared in 0.05 M KOH provided effective protection from corrosion for magnesium alloys.

## 1. INTRODUCTION

Magnesium and its alloys have attracted a lot of attention due to their superior properties [1–4], such as mechanical properties, which are close to human bones and have remarkable biocompatibility. However, Mg alloys degrade too rapidly in physiological environments [5–7]. Many surface modification treatments have been developed that provide quite effective protections for Mg alloys. Micro-arc oxidation (MAO) is the most promising strategy for retarding the degradation rate of Mg

alloys [8–11]. Advantages, including good adhesion of coatings to the substrate, easy control, environmentally-friendly processing, and low cost, have made this approach valuable.

To date, the characteristics of MAO coatings have been investigated and found to be influenced significantly by the process parameters [12–14], electrolyte [15–17], and substrate chemical composition [18–21]. Once the substrate materials and process parameters are fixed, the electrolyte is crucial to MAO coating properties. The concentration and chemical composition of electrolytes influence MAO coating morphology, such as pore size, shape and distribution, coating formation kinetics and composition, and substrate corrosion protection. Choosing the correct electrolyte can reduce coating micropores and microcracks [22] and, consequently, enhance corrosion protection for Mg alloys. Dou has fabricated MAO coatings in silicate and calcium phosphate-based electrolytes on Mg-1.74Zn-0.55Ca alloys [23], and found that CaP-containing MAO coatings more sufficiently protect magnesium alloys from corrosion in long-term immersions. Similarly, Ghasemi have studied the influence of different electrolytes, including $Na_2SiO_3$, $Na_3PO_4$, and $NaAlO_2$, with KOH addition on MAO coatings on AM50 alloys [22]. Results have indicated that MAO coatings obtained in $Na_2SiO_3$ electrolyte show better corrosion resistance from the formation of a thicker coating with less porosity. Notably, it has been found that an alkaline electrolyte is commonly applied in the MAO process for magnesium alloys while metal dissolution occurs in acid electrolytes. Li have studied the influence of NaOH addition in electrolytes on coating chemical composition, surface morphology, and corrosion resistance [24]. They found that NaOH addition promoted the formation of uniform and stable coatings and resulted in great improvements in corrosion protection for Mg substrates. However, defects, such as microcracks and micropores, still hinder corrosion protection by MAO coatings for magnesium alloys. Therefore, the goal of this study was to determine the correct electrolyte for modifying surface morphology to enhance coating corrosion protection.

In this study, phosphate-borate electrolytes with different KOH content were used to fabricate MAO coatings on ZK60 Mg alloys. Borate addition has been reported to result in MAO coating formation with high microhardness and good crystallinity [25]. Also, borates accelerated coating formation by providing oxygen through decomposition. It has been suggested that, with increased KOH concentration, electrolyte conductivity and viscosity increase and the ignition/breakdown voltage decreases, thereby generating homogeneous MAO coatings with large corrosion resistance [26–27]. Thus, in this study, the effects of KOH concentrations on the microstructure and corrosion resistance of MAO coatings on ZK60 Mg alloys were investigated in detail.

## 2. EXPERIMENTAL

### 2.1. Preparation of MAO coatings

Samples were fabricated from an alloy ingot of ZK60 Mg alloy. First, 20×20×5 mm samples were cut and provided a smooth surface by grinding and polishing with SiC abrasive papers (to mesh 2000). A 1.5 mm-diameter hole was drilled in one side of the samples to ensure the stable current passing into the specimens and solution.

Micro-arc oxidation was conducted with a high-power pulsed WHD-20 bi-polar electrical source. The electrolyte was prepared using $Na_3PO_4$ (0.05 M) and $Na_2B_4O_7$ (0.02 M) in distilled water

with KOH at different concentrations (0.01, 0.05, and 0.1 M). The MAO process was carried out for 15 min at room temperature in a water-cooled stainless steel tank. The anode was the submersed magnesium substrate and the counter electrode the stainless steel tank. The electrical parameters, including a positive constant voltage, negative constant voltage, duty cycle, and pulse frequency, were 350 V, 20 V, 30%, and 600 Hz, respectively. Finally, MAO-coated samples were rinsed in distilled water and ethanol and dried in air at room temperature.

## 2.2. Characterization of MAO coatings

The surface and cross-section morphologies of MAO coatings were characterized using a scanning electron microscope (SEM, Quanta 200 FEG, FEI Company, Hillsboro, OR, USA). The phase structure of the coating was investigated by X-ray diffraction (DX-2700, Fangyuan, Dandong, China) with Cu-Kα radiation at a scanning speed of 0.03°/s.

## 2.3. Electrochemical measurements

Electrochemical measurements were conducted using a standard three-electrode cell (CHI600, CH Instruments, Shanghai, China). A saturated calomel act was the reference electrode, the counter electrode graphite, and the sample the working electrode. The experimental temperature was held kept at 37 ±0.5° C and the area of the working electrode at 20×20 mm. A simulated body fluid solution (SBF, composition in Table 1) was used as the electrolyte for potentiodynamic polarization studies, which were performed from -2 to 0 V and at a scanning rate of 0.5 mV/s. Electrochemical impedance spectroscopic (EIS) experiments were performed with an open circuit potential with an AC amplitude of 5 mV in a frequency range varying from $10^5$ to $10^{-2}$ Hz. Prior to measurement, samples were immersed in SBF for 20 min to maintain a stable open potential.

## 2.4 Immersion test

Immersion tests were performed to evaluate the biodegradability *in vitro* of these samples. The pH was 7.4 ±0.2, and temperature 37 ±0.5° C, with the use of a water bath, and samples immersed in 100 ml of SBF for 14 d. During immersion tests, the solution pH and sample weights were recorded every 48 h. A blank SBF was used as the control.

**Table 1.** Chemical composition of the simulated body fluid (SBF) solution

| Components | Concentration(g/L) |
|---|---|
| NaCl | 8.0 |
| $CaCl_2$ | 0.14 |
| $MgCl_2 \cdot 6H_2O$ | 0.1 |
| $NaHCO_3$ | 0.35 |
| Glucose | 1.0 |
| KCl | 0.4 |
| $Na_2HPO_4 \cdot 2H_2O$ | 0.06 |
| $MgSO_4 \cdot H_2O$ | 0.06 |
| $KH_2PO_4$ | 0.06 |

## 3. RESULTS AND DISCUSSION

### 3.1. Effects of KOH concentrations on the composition of the MAO coatings
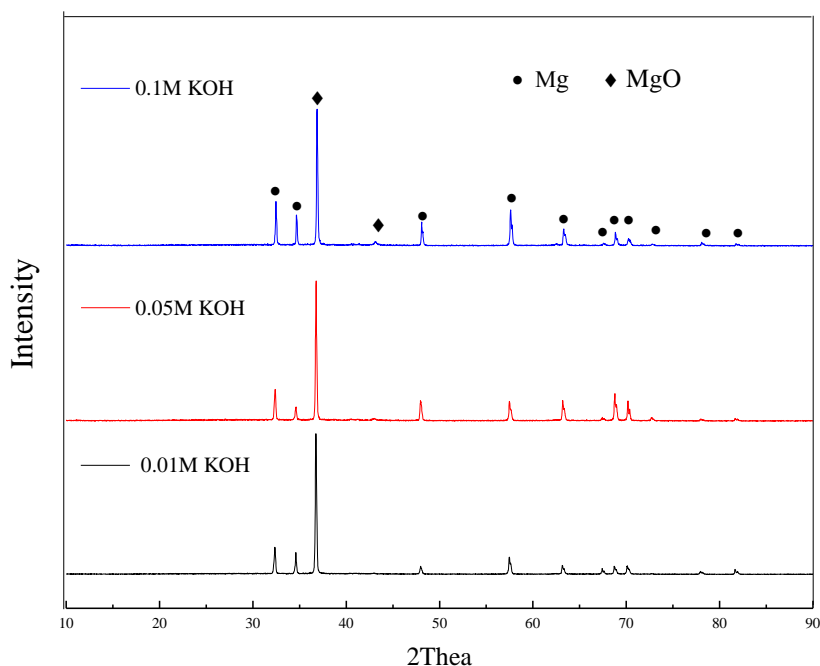


**Figure 1.** XRD patterns of the MAO coatings prepared in different KOH concentrations (0.01M, 0.05M and 0.1M)

XRD results from ZK60 Mg alloys with MAO coatings fabricated at different KOH concentrations showed clearly that the main component of the coatings was the MgO phase (Fig. 1), without any other impurities, such as $Mg_3(PO_4)_2$ phase, in the coatings [28–30], which was in agreement with the results obtained by Liang [31] and Lee [32]. During the MAO process, borate offers oxygen, from $B_4O_7^{2-}$ decomposition, for reactions with metal cations in the electric field, resulting in rapid growth of the oxide layer on ZK60 substrates [33]. In this micro-arc oxidation process, various possible reactions occurred as follows

$Mg \rightarrow Mg^{2+} + 2e^-$ （1）

$4OH^- \rightarrow O_2\uparrow + 2H_2O + 4e\text{-}$ （2）

$2H_2O \rightarrow 2H_2\uparrow + O_2\uparrow$ （3）

$2Mg + O_2 \rightarrow 2MgO\downarrow$ （4）

$Mg^{2+} + OH^- \rightarrow Mg(OH)_2\downarrow$ （5）

$Mg(OH)_2 \rightarrow MgO\downarrow + H_2O$ （6）
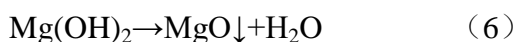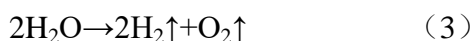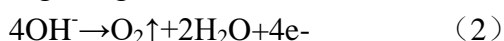
The relative contents of MgO phase in MAO coatings were investigated by evaluating the relative intensity ($I_{MgO}/I_{Mg}$) of the MgO and Mg phases from XRD patterns. The relative intensities were found to be 6.7, 10.8, and 4.6 for MAO coatings prepared in 0.01, 0.05, and 0.1 M KOH, respectively, with the MgO phase content the highest in 0.05 M KOH.

*3.2. Effects of KOH concentrations on the surface and cross-sectional morphologies*
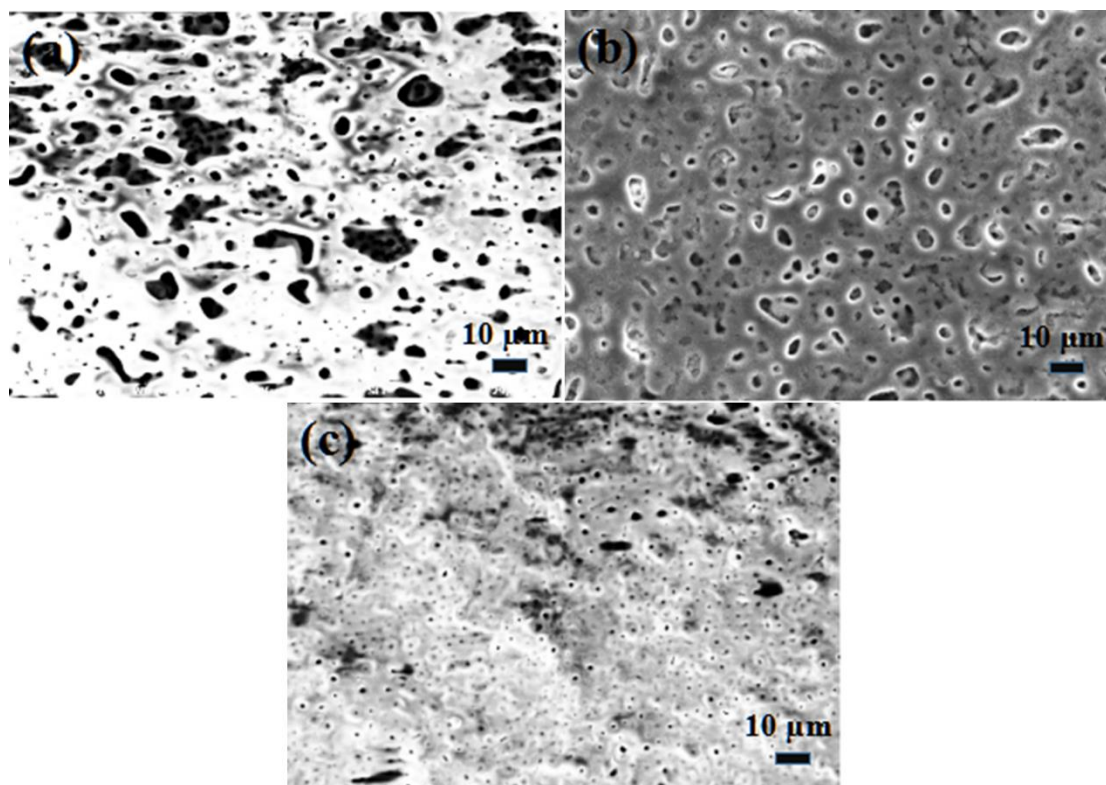


**Figure 2.** SEM micrographs of the MAO coatings prepared in varied KOH concentrations（a–c: 0.01, 0.05, and 0.1 M KOH, respectively）

The surface morphologies of MAO coatings prepared in various KOH concentrations showed that cracks and pores were distributed on the coatings, forming a rough surface (Fig. 2). The oxide melted and gas was released from micro-arc oxidation discharge channels, resulting in pore formation [34]. Also, fast cooling molten oxides in the electrolyte at a relatively low temperature contributed to the generation of thermal stresses inside oxide films, and microcracks formed due to stress relief. Rough coating surfaces were ascribed to alternating melting and sintering. However, nearly no visible microcracks existed in MAO coating fabricated in 0.05 M KOH, while many more cracks were found in the surfaces of the other two samples.

From the cross-sectional morphologies of MAO coatings fabricated in various KOH concentrations, it was inferred that electric spark discharge dominated the MAO process because of the existence of melts (Fig. 3). In addition, MAO coatings were clearly all composed of two layers: an inner compact layer and an outer layer with pores.

Based on the surface and cross-sectional morphologies of these MAO coatings, the thicknesses, pore diameters, pore sizes of MAO coatings at different KOH concentrations were estimated (Table 2). The pore size and coating thickness were observed to decrease as KOH concentration increased from 0.01 to 0.1 M, but the porosity was the lowest ($5.156 \times 10^{-3}$ pores/$\mu m^2$) in 0.05 M KOH. Also, Figure 2 clearly showed that the pore distribution of a micro-arc oxidation coating obtained in 0.05 M KOH was relatively uniform. Increased KOH concentration increased conductivity [35], which led to increased

appearances of different spark features, including electric spark discharge frequency, size, and number of sparks that occurred in the spark discharge process of micro-arc oxidation. This resulted in a large number of microcracks and micropores on the MAO coatings [36].
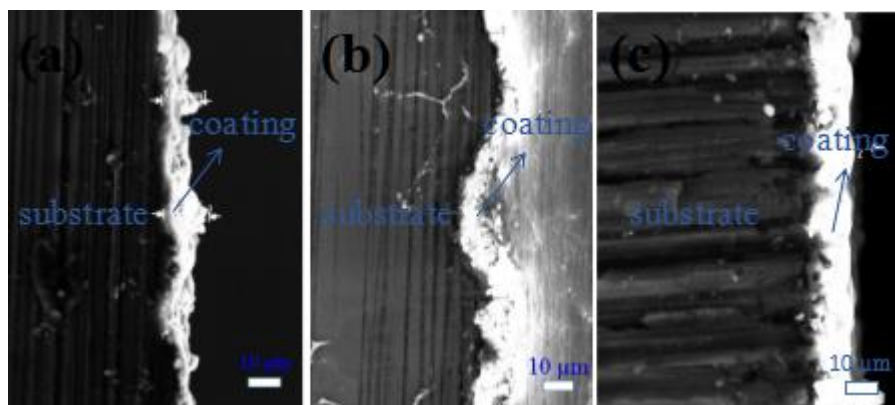


**Figure 2.** Cross-sectional morphologies of the MAO coatings prepared in different KOH concentrations（a–c: 0.01, 0.05, and 0.1 M KOH, respectively）

**Table 2.** Characteristics of the MAO coatings fabricated in different KOH concentrations

| Electrolyte | Thickness of coating (μm) | Pore diameter (μm) | Porosity ($\times 10^{-3}$ pores/$\mu m^2$) |
|---|---|---|---|
| 0.01M KOH | 13.20 | 6.00 | 8.13 |
| 0.05M KOH | 8.82 | 3.33 | 5.16 |
| 0.1M KOH | 7.40 | 1.75 | 15.00 |

*3.2. Effects of KOH concentration on the corrosion resistance of the MAO-coated ZK60 alloys*

The potentiodynamic polarization curves of MAO-coated ZK60 alloys prepared at different KOH concentrations are shown in Figure 4. The anodic Tafel slope ($\beta_a$), cathodic Tafel slope ($\beta_c$), corrosion current density ($I_{corr}$), corrosion potential ($E_{corr}$), corrosion rate ($P_i$), and polarization resistance [37] ($R_p$) values are compiled in Table 3. As the KOH concentration in the electrolyte increased, the self-corrosion potential of coated samples increased from -1.53 to -1.17 V, indicating a decreased probability of corrosion susceptibility for samples prepared by micro-arc oxidation. However, at the same time, with increased KOH concentration, the self-corrosion current density of coated samples did not correspondingly decrease but increased to some extent, which indicated that the corrosion rate of MAO-coated samples increased. It was also observed that, as the KOH concentration decreased, the corrosion rate of coated samples decreased from $3.51 \times 10^{-5}$ to $1.00 \times 10^{-5}$ mm·yr$^{-1}$ and the polarization resistance increased more than 4-fold. This meant that changing the KOH concentration helped enhance the corrosion resistance of MAO-coated ZK60 samples. According to the results, it was clear that coatings fabricated in 0.05 M KOH exhibited the best corrosion resistance. This was due

to the good surface quality of micro-arc oxidation coatings prepared in 0.05 M KOH, which produced the lowest porosity, uniform pore size, no microcracks, and highest MgO phase content.
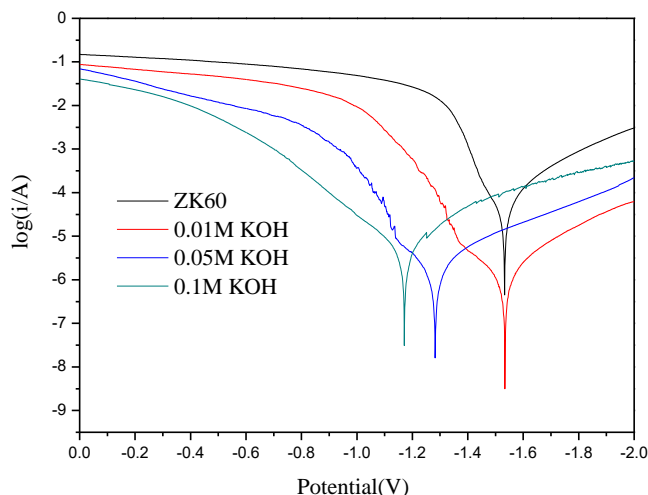


**Figure 4.** Potentiodynamic polarization curves of the MAO coatings prepared in different KOH concentrations

**Table 3.** Electrochemical corrosion properties of coating samples

| Samples | $\beta_a$ (V·dec$^{-1}$) | $\beta_c$ (V·dec$^{-1}$) | $E_{corr}$ (V) | $I_{corr}$ (A·cm$^{-2}$) | $R_p$ (k$\Omega$·cm$^2$) | $P_i$ (mm·year$^{-1}$) |
|---|---|---|---|---|---|---|
| ZK60 | 5.97 | 14.53 | -1.53 | 8.66E-06 | 212.3 | 1.98E-04 |
| 0.1M KOH | 3.91 | 5.66 | -1.17 | 1.53E-06 | 654.4 | 3.51E-05 |
| 0.05M KOH | 5.64 | 5.10 | -1.28 | 4.36E-07 | 2667.2 | 1.00E-05 |
| 0.01M KOH | 5.72 | 5.47 | -1.53 | 4.69E-07 | 2587.8 | 1.07E-05 |
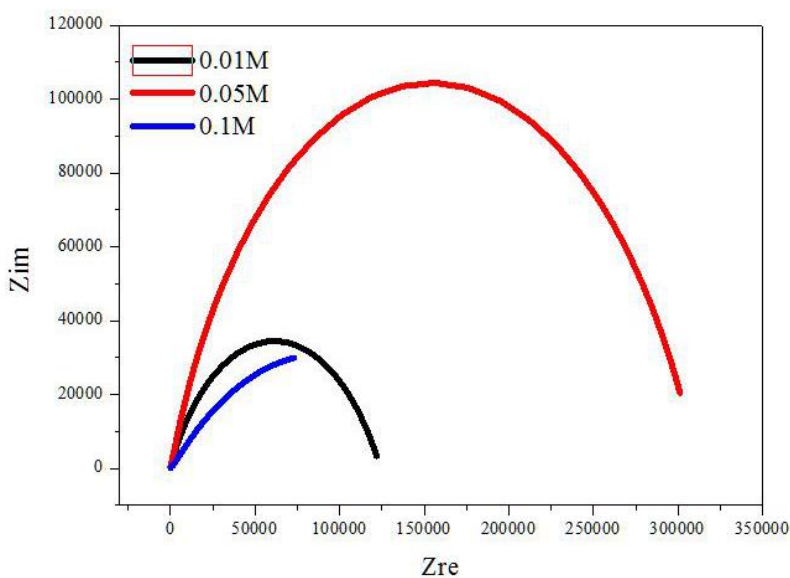


**Figure 5.** Nyquist plots of the MAO coatings prepared in different KOH concentrations
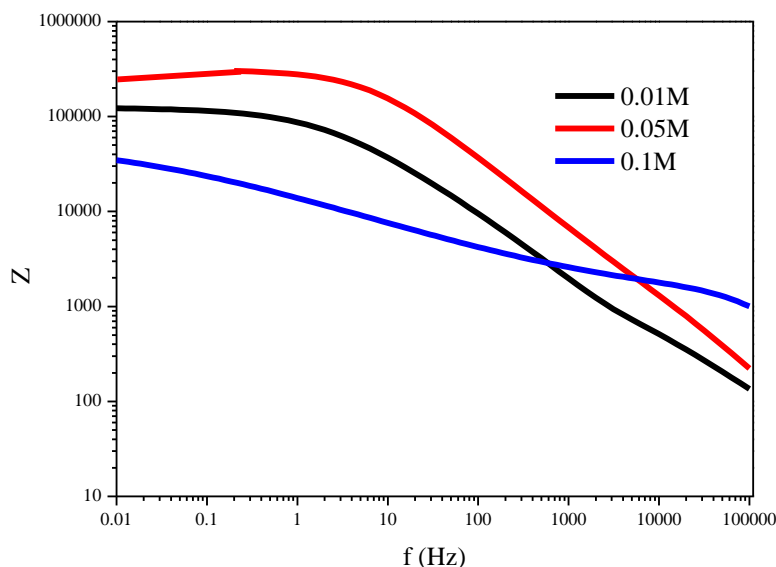
**Figure 6.** Bode plots of the MAO coatings prepared in different KOH concentrations
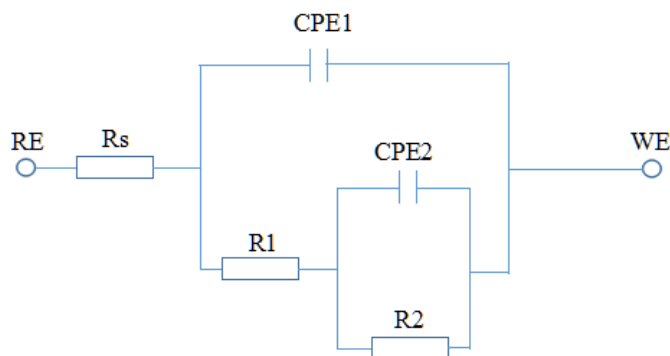


**Figure 7.** Equivalent circuit for fitting the EIS plots of the MAO coatings prepared in different KOH concentrations

Nyquist plots of samples prepared by micro-arc oxidation in different KOH concentrations in SBF showed that the diameter of the impedance arc of MAO coatings prepared in 0.05 M KOH was significantly larger than that of the other samples (Fig. 5), indicating that its corrosion impedance was the greatest. The Bode plot of MAO coatings on ZK60 alloy samples prepared in different KOH concentrations showed that the impedance of all samples decreased with increased frequency over the range of 0.01–100000 Hz (Fig. 6). MAO-coated samples prepared in 0.05 M KOH exhibited the highest impedance in almost the whole frequency range. A model was proposed to fit the EIS plots [38], in which Rs represented the solution resistance, $R_1$ the resistance of outer coating layer in parallel with constant phase element $CPE_1$, which was exposed to the corrosive solution, and $R_2$ in parallel with $CPE_2$ the resistance of the inner coating layer, including that of the coating/substrate interface (Fig. 7) [39,40]. According to the above equivalent circuit fitting, the fitting values of each circuit element in each sample in SBF are shown in Table 4. The impedance of each sample was mainly derived from the charge transfer resistor $R_2$, which was ~2 to 3 orders of magnitude higher than that of

the outer porous layer $R_1$ and one order of magnitude higher than that of the ZK60 alloy substrate ($\sim 1.414 \times 10^4$ $\Omega \cdot cm^2$). Reducing the KOH concentration led to decreased electrolyte conductivity and reduced spark discharge on substrate surfaces, which contributed to the formation of micro-arc oxidation coatings with fewer surface pores and cracks. The sample prepared by micro-arc oxidation in 0.05 M KOH exhibited the lowest porosity, uniform pore distribution, and nearly no microcracks, which effectively prevented substrate erosion caused by infiltration of corrosive fluids into the pores, thus protected the magnesium alloy. These results were consistent with previous electrochemical polarization data.

**Table 4.** Fitting results of the MAO coatings for EIS plots from Figures 4 and 5

| Samples | Rs ($\Omega cm^2$) | (CPE-T)$_1$ | $n_1$ | $R_1$ ($\Omega cm^2$) | (CPE-T)$_2$ | $n_2$ | $R_2$ ($\Omega cm^2$) |
|---|---|---|---|---|---|---|---|
| 0.1M KOH | 77.69 | 1.50E-7 | 0.80 | 918.7 | 2.57E-5 | 0.43 | 1.77E5 |
| 0.05M KOH | 662.3 | 5.32E-8 | 0.85 | 3337 | 1.59E-7 | 0.70 | 3.09E5 |
| 0.01M KOH | 1.01 | 1.52E-6 | 0.63 | 2649 | 2.06E-8 | 1.00 | 1.22E5 |

### 3.4. Effects of KOH concentration on immersion degradation behavior

The biodegradability of MAO-coated samples was evaluated through immersion tests *in vitro,* conducted in SBF at 37° C for 14 d. The results showed that the weight loss and pH changed with immersion time for MAO-coated samples prepared in different KOH concentration (Fig. 8), while mass loss did not change significantly with immersion time. For pH versus time curves, all MAO-coated samples exhibited increased pH with increased immersion time.
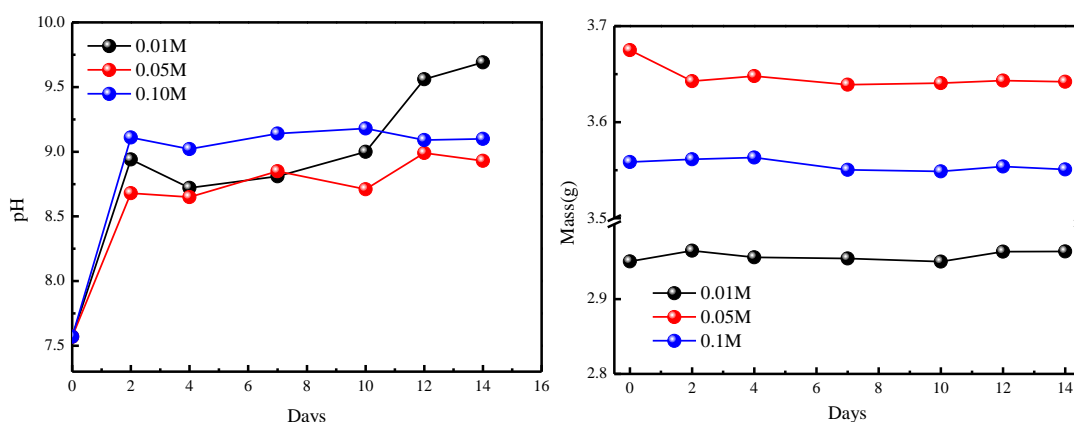


**Figure 8.** Immersion test results of the MAO coatings prepared in different KOH concentrations: pH (left) and mass values (right)

In the initial immersion stage, pH increased rapidly, which was attributed to the presence of porous surface layer, and SBF began to enter pores, giving rise to coating surface corrosion and rapid increases in pH. After that, the $Mg^{2+}$ concentration increased, accompanied by increased $OH^-$, which

caused magnesium hydroxide deposition. Then, deposition covered the sample surface and hindered continued corrosion by corrosive ions, but the magnesium hydroxide amounts were not very large. With infiltration of corrosive SBF, pores in a coating's outer porous layer slowly expanded, such that the SBF entered the outer pores to the coating's inner dense layer, thus reaching the interface between the substrate and dense layer. However, a long time was needed to infiltrate to the interface from the outer surface layer, which was explained by the protective effect of MAO coatings on the alloy coming mainly from the inner dense layer. At the same time, calcium phosphates began to deposit in large quantities, eventually stabilizing the pH.

## 4. CONCLUSION

Different MAO coatings were fabricated on ZK60 magnesium alloys in phosphate-borate electrolyte with different KOH concentrations. XRD results indicated that only the MgO phase without any other impurities existed in all MAO coatings. The KOH concentration had great influence on coating surface morphologies and the corrosion current density of MAO-coated alloys decreased about one order of magnitude more than that of than untreated substrates. The MAO-coated sample treated in 0.05 M KOH showed a relatively high self-corrosion potential, highest polarization resistance, lowest corrosion current density, and low corrosion rate, indicating the best corrosion resistance among all samples. The results from immersion tests also suggested that MAO coatings obtained in 0.05 M KOH displayed superior corrosion resistance in SBF *in vitro*. This good corrosion *in vitro* was mainly ascribed to the good surface quality of these MAO coatings.

**References**

1. S. Virtanen, *Mater. Sci. Eng*. B, 176 (2011) 1600.
2. M. Laleh, A. S. Rouhaghdam, T. Shahrabi, A. Shanghi, *J. Alloys Compd.*, 496 (2010) 548.
3. S. L. Aktu, S. Durdu, I. Kutbay, M. Usta, *Ceram. Int.*, 42 (2015) 1246.
4. S. Agarwal, J. Curtin, B. Duffy, & S. Jaiswal, *Materials Science and Engineering C*, 68 (2016) 948.
5. K. Xia, H. Pan, T. Wang, S. Ma, J. Niu, Z. Xiang, Y. Song, H. Yang, X. Tang, W. Lu, M*aterials Science and Engineering C,* 72 (2017) 676.
6. H. Yang, K. Xia, T. Wang, J. Niu, Y. Song, Z. Xiong, K. Zheng, S. Wei, W. Lu, *J. Alloys Compd.*, 672 (2016) 366.
7. A. Atrens, G. Song, M. Liu, Z. Shi, F. Cao, and M. S. Dargusch, *Adv. Eng. Mater.*, 17 (2015) 400.
8. U. Malayoglu, K. C. Tekin, S. Shrestha, *Surf. Coat. Technol.*, 205 (2010) 1793.
9. Z. P. Yao, L. L. Li, X. R. Liu, Z. H. Jiang, *Surf. Eng.*, 26 (2010) 317.
10. X. G. Han, X. P. Zhu, M. K. Lei, *Surf. Coat. Technol.*, 206 (2011) 874.
11. Y. Gu, C. F. Chen, S. Bandopadhyay, C. Ning, Y. Zhang, Y. Guo, *Appl. Surf. Sci.*, 258 (2012)

6116.

12. R. F. Zhang, D. Y. Shan, R. S. Chen, E. H. Han, Materials Chemistry and Physics 107 (2008) 356.
13. Z. Li, Y. Yuan, X. Jing, *Journal of Alloys and Compounds*, 541 (2012) 380.
14. V. Ezhilselvi, J. Nithin, J.N. Balaraju, S. Subramanian, *Surface & Coatings Technology*, 288 (2016) 221.
15. R. F. Zhang, S. F. Zhang, J. H. Xiang, L. H. Zhang, Y. Q. Zhang, S. B. Guo, *Surf. Coat. Technol*., 206 (2012) 5072.
16. L. R. Krishna, G. Poshal, G. Sundararajan, *Metal. Mater. Trans*. A, 41 (2010) 3499.
17. R.F. Zhang, G.Y. Xiong, C.Y. Hu, Curr. *Appl. Phys*., 10 (2010) 255.
18. S. Q. Wang, F. Q. Xie, X. Q. Wu, *Materials Chemistry and Physics*, 202 (2017) 114.
19. D. Salih, K. Kemal, S.L. Aktuğ, A. Çakır, *Surface & Coatings Technology*, 326 (2017) 111.
20. S. X. He, Y. L. Ma, H. Yeb , X. D. Liu, Z. Y. Dou, Q. D. Xu, H. J. Wang, P. C. Zhang, *Corrosion Science*, 122 (2017) 108.
21. F. Simchen, M. Sieber, T. Lampke, *Surface & Coatings Technology*, 315 (2017) 205.
22. A. Ghasemi, V. S. Raja, C. Blawert, W. Dietzel, & K. U. Kainer, *Surf. Coat. Technol*., 204 (2010) 1469.
23. J. Dou, G. Gu, C. Chen and Y. Pan, *RSC Adv*., 994 (2016) 104808.
24. L. Li, T. S. N. Sankara Narayanan, Y. K. Kim, J. Y. Kang, I. S. Park, T. S. Bae & M. H. Lee, *Surf. Interface Anal*., 46 (2014) 7.
25. H. X. Li, V. S. Rudnev, X. H. Zheng, T. P. Yarovaya and R. G. Song, *J. Alloys Compd*., 462 (2008) 99
26. Y. G. Ko, S. Namgung, D. H. Shin, *Surf. Coat. Technol*., 205 (2010) 2525
27. Y. L. Cheng, T. W. Qin, L. L. Li, H. M. Wang, Z. Zhang, *Corros. Eng. Sci. Technol*., 46 (2011) 17
28. A. Seyfoori, S. Mirdamadi, A. Khavandi, Z. S. Raufi, *Appl. Surf. Sci*., 261 (2012) 92.
29. S. Durdu, M. Usta, *Appl. Surf. Sci*., 261 (2012) 774.
30. S. Yagi, A. Sengoku, K. Kubota, E. Matsubara, *Corros. Sci*., 57 (2012) 74.
31. J. Liang, P. B. Srinivasan, C. Blawert, W. Dietzel, *Corros. Sci*., 51 (2009) 2483.
32. K. M. Lee, Y. G. Ko, D. H. Shin, *J. Alloys Compd*., 615 (2014) S418.
33. R. F. Zhang, S. F. Zhang, Y. L. Shen, L. H. Zhang, T. Z. Liu, Y. Q. Zhang, S. B. Guo, *Appl. Surf. Sci.*, 258 (2012) 6602.
34. F. Liu, J. L. Xu, F. P. Wang, L. C. Zhao and T. D. Shimizu, *Surf. Coat. Technol*., 204 (2010) 3294.
35. S. B. Guo, Y. Q. Zhang, R. F. Zhang, S. F. Zhang, H. H. Zhang, *Mater. Chem. Phys*., 141 (2013) 121.
36. J. Liang, P. B. Srinivasan, C. Blawert, M. Störmer, W. Dietzel, *Appl. Surf. Sci*., 255 (2009) 4212.
37. M. Stern, A. L. Geary, J. Electrochem. Soc., 104 (1957) 56.
38. Y. Gu, C.-f. Chen, S. Bandopadhyay, C. Ning, Y. Zhang, Y. Guo, *Appl. Surf. Sci*., 258 (2012) 6116.
39. L. Pezzato, K. Brunelli, E. Napolitani, M. Magrini, M. Dabalà, *Appl. Surf. Sci.,* 357 (2015) 1031.
40. F. Muhaffel, F. Mert, H. Cimenoglu, D. Höche, M. L. Zheludkevich, C. Blawer, *Surf. Coat. Technol*., 269 (2015) 200.